ORGANOMETALLIC AMINOMETHYL 1,2,3-TRIAZOLES: SYNTHESIS, CHARACTERIZATION AND REACTIVITY

LUIS PEÑA [a], DAVID VILLAMAN [a], AND RODRIGO ARANCIBIA [a]*

[a] *Facultad de Ciencias Químicas, Universidad de Concepción, Concepción, Chile.*

ABSTRACT

In search of new organometallic-1,2,3-triazoles, this work describes a convenient synthesis to obtain ferrocenyl and cyrhetrenyl 1,2,3-triazole derivatives containing aminomethyl fragment. On this regard, the compounds of general formulae [(η^5-C_5H_4-(1)-1,2,3-triazole-(4)-CH_2NH_2)MLn] [where MLn =Fe(η^5-C_5H_5) (**1a**), Re(CO)$_3$ (**1b**)] were obtained via *tert*-butoxycarbonyl (BOC) deprotection under acid conditions of the corresponding protected triazoles [(η^5-C_5H_4-(1)-1,2,3-triazole-(4)-$CH_2NH(C{=}O)OC(CH_3)_3$)MLn] with MLn = Fe(η^5-C_5H_5) (**P1**), Re(CO)$_3$ (**P2**)], with good yields (89–95%). In addition, the reactivity of aminomethyl compounds (**1a**–**b**) was evaluated in condensation reactions with 4-(1H-1,2,4-triazol-1-yl)benzaldehyde, isolated the Schiff bases [(η^5-C_5H_4-(1)-1,2,3-triazole-(4)-$CH_2N{=}CH$-(1)-C_6H_4-(4)-1H-1,2,4-triazole)MLn] (**2a**–**b**) [where MLn =Fe(η^5-C_5H_5) (**2a**), Re(CO)$_3$ (**2b**)] under mild reactions conditions. All compounds were characterized by FT-IR, ^{1}H NMR spectroscopy and elemental analysis. Moreover, the molecular structure of **2a** was determined by single-crystal X-ray diffraction.

Keywords: Organometallic-1,2,3-triazole, Cyrhetrene, Ferrocene, Aminomethyl, Reactivity.

1. INTRODUCTION

Organometallic compounds, characterized by at least one metal–carbon bond, constitute a highly versatile class of chemical systems [1]. Their ability to combine the electronic properties of transition metals with the structural diversity of organic frameworks enables precise tuning of reactivity and redox behavior [2], supporting a wide range of applications in catalysis [3], materials science [4], and medicinal chemistry [5–10].

Among the various organometallic architectures, metallocenes and half-sandwich complexes are particularly valued for their remarkable stability and tunable electronic properties [11–13]. Notably, ferrocene [(η^5-C_5H_5)Fe(η^5-C_5H_5)] and cyrhetrene [(η^5-C_5H_5)Re(CO)$_3$] entities exhibit complementary electronic characteristics, with ferrocene acting as an efficient electron donor group and cyrhetrene as an electron acceptor group. This donor–acceptor duality has been widely explored in the design of ferrocenyl and cyrhetrenyl derivatives bearing diverse heterocyclic or functionalized organic fragments, where incorporation of these organometallic units enables systematic modulation of redox behavior, physicochemical properties, and biological activity [14–18].

Furthermore, these organometallic moieties have been successfully integrated into biologically active scaffolds through 1,2,3-triazole linkers using Cu(I)-catalyzed azide–alkyne cycloaddition (CuAAC), providing a powerful and versatile synthetic approach to enhance both chemical diversity and bioactivity [19–24]. For instance, Bieganski and co-workers recently synthesized ferrocene–1H-1,2,3-triazole-3′-azido-3′-deoxythymidine (AZT) hybrids, which exhibited enhanced anticancer activity against A549 and H1975 NSCLC cells [25].

A particularly valuable extension of this approach involves the use of BOC-protected aminomethyl alkynes. The CuAAC reaction of these derivatives with azides selectively affords protected 1,2,3-triazole hybrids, temporarily masking the aminomethyl functionality [26]. Upon deprotection, the aminomethyl group is revealed as a highly reactive nucleophile capable of undergoing condensation with carbonyl-containing fragments, including biologically relevant units such as 1,2,4-triazoles. This modular, stepwise strategy enables the rapid formation of Schiff bases, facilitating the incorporation of diverse functional motifs and expanding the chemical and structural diversity of organometallic hybrids [27].

For other hand, 1,2,4-triazoles cores have also been extensively employed owing to their favorable electronic and structural properties, which enhance chemical stability and intermolecular interaction capabilities [28–33]. Recently, Yin and collaborators reported the synthesis of novel organic analogues comprising 1,2,4-triazole Schiff bases hybridized with 1,4-naphthoquinones. These chiral 1,2,4-triazole derivatives exhibited notable anticancer activity against HeLa cells, achieving IC_{50} values as low as 1.8 μM for the most active compound. To the best of our knowledge, organometallic Schiff bases incorporating 1,2,4-triazole scaffolds have been have not been extensively studied with anticancer applications [34]. Particularly, aminomethyl-1,2,3-triazole organometallic complexes have not been explored as condensation precursors. On this regard, in this work, we report the design of such derivatives, which efficiently condense with 1,2,4-triazole aldehydes to yield Schiff bases. The pronounced nucleophilicity of their aminomethyl groups underscores their reactivity and highlights their potential as versatile scaffolds for the development of organometallic–organic hybrid systems.

2. EXPERIMENTAL SECTION

2.1. Reagents and methods

All manipulations were conducted under an N_2 atmosphere using Schlenk techniques. The compounds [(η^5-C_5H_4-(1)-1,2,3-triazole-(4)-CH_2-NH-C=(O)$OC(CH_3)_3$)Fe(η^5-C_5H_5)] (**P1**) and [(η^5-C_5H_4-(1)-1,2,3-triazole-(4)-CH_2-NH-C=(O)$OC(CH_3)_3$)Re(CO)$_3$] (**P2**) were prepared according to published procedures [35]. 4-(1H-1,2,4-Triazol-1-yl)benzaldehyde (97%), and Trifluoroacetic acid (TFA) (≥98.0%) were obtained from Ambeed and Sigma-Aldrich, respectively. Solvents such as CH_2Cl_2 (DCM), hexane, acetone, MeOH, DMSO and THF were obtained commercially and purified using standard methods [36]. Infrared spectra were recorded in solid state (KBr pellet) on a Jasco FT-IR 4600 spectrophotometer. NMR spectra were measured on a Bruker spectrometer model ASCEND TM 400 MHz. All NMR spectra are reported in parts per million (ppm, δ) relative to tetramethylsilane (Me_4Si), with the residual solvent proton resonances used as internal standards. Coupling constants (*J*) are reported in Hertz (Hz), and integrations are reported as number of protons. The following abbreviations were used to describe the peak patterns: s = singlet, d = doublet, t = triplet, and m = multiplet.

2.2. General procedure for BOC Deprotection under acidic conditions (1a–b)

In a 100 mL round-bottom two-neck flask, 1 equivalent of [(η^5-C_5H_4-(1)-1,2,3-triazole-(4)-CH_2NH-C=(O)$OC(CH_3)_3$)MLn] with MLn = Fe(η^5-C_5H_5) (**P1**), Re(CO)$_3$ (**P2**), was dissolved in 5 mL of dry dichloromethane (DCM). The solution was cooled to 0 °C, and 15 mL of a 50% DCM/trifluoroacetic acid (TFA) mixture was added dropwise over 10 min. Upon completion of the addition, the cooling bath was removed, and the reaction was stirred at room temperature for 2–3 hours. The reaction was monitored by thin-layer chromatography (TLC). After completion, the reaction mixture was concentrated under reduced pressure and redissolved in DCM (3 × 5 mL). The solution was then neutralized in a separatory funnel with a 20% aqueous $NaHCO_3$ solution, followed by two additional washes with distilled water. The organic layer was separated, and the final mixture was dried under vacuum and subsequently purified by column chromatography on SiO_2 using a DCM/MeOH (7:3) eluent.

*[(η^5-C_5H_4-(1)-1,2,3-triazole-(4)CH_2-NH_2)Fe(η^5-C_5H_5)] (**1a**)*

This compound was prepared according to the general procedure described above, using in this case: [(η^5-C_5H_4-(1)-1,2,3-triazole-(4)-CH_2-NH-C=(O)$OC(CH_3)_3$)Fe(η^5-C_5H_5)] (**P1**) (200 mg, 0.523 mmol). Orange solid, yield 95% (140 mg, 0.497 mmol).

*Corresponding author email: rarancibia@udec.cl

FT-IR (KBr, cm^{-1}): 3288 (νN–H); 1655 (νN–H bend); 1609 (νC=N); 1521 (νC=C). ^1H NMR (DMSO-d_6): δ 8.33 (s, 1H, 1,2,3-triazole); 4.99 (t, J = 2.0 Hz, 2H, C_5H_4); 4.34 (t, J = 2.0 Hz, 2H, C_5H_4); 4.22 (s, 5H, C_5H_5); 3.80 (s, 2H, CH_2); 1.95 (s, 2H, NH_2). Anal. (%) Calc. for $C_{13}H_{14}FeN_4$: C, 55.34; H, 5.00 and N, 19.86; found: C, 15.03; H, 4.13 and N, 15.03.

*[(η^5-C_5H_4-(1)-1,2,3-triazole-(4)CH_2-NH_2)Re$(CO)_3$] (**1b**)*

This compound was prepared according to the general procedure described above, using in this case: [(η^5-C_5H_4-(1)-1,2,3-triazole-(4)-CH_2-NH-C=(O)OC$(CH_3)_3$)Re$(CO)_3$] (**P2**) (250 mg, 0.470 mmol). Green solid, yield 89% (181 mg, 0.418 mmol). FT-IR (KBr, cm^{-1}): 3288 (νN–H); 3122 (νCsp²–H); 2028 (νRe-C=O); 1911 (νRe-C=O); 1678 (νN–H bend); 1527 (νC=C). ^1H NMR (DMSO-d_6): δ 8.43 (s, 1H, 1,2,3-triazole); 6.55 (t, J = 2.4 Hz, 2H, C_5H_4); 5.80 (t, J = 2.4 Hz, 2H, C_5H_4); 3.80 (s, 2H, CH_2); 1,98 (s, 2H, NH_2). Anal. (%) Calc. for $C_{11}H_{14}FeN_4O_3$: C, 30.62; H, 2.10 and N, 12.99; found: C, 29.70; H, 2.50 and N, 12.46.

2.3. General procedure for the synthesis of organometallic-1,2,3/1,2,4-triazole Schiff Bases (2a–b)

In a Schlenk tube under a nitrogen atmosphere, equimolar amounts of the organometallic aminomethyl-1,2,3-triazole derivative (**2a**–**b**) and 4-(1H-1,2,4-triazol-1-yl)benzaldehyde were combined. The tube was evacuated and backfilled with N_2 (three cycles), and anhydrous dichloromethane (10 mL) was added via syringe. The reaction mixture was stirred at room temperature for 30 min before adding solid Na_2SO_4. The mixture was then allowed to stir at room temperature for an additional 4–16 h, while the progress of the reaction was monitored by TLC, following the disappearance of the aminomethyl starting material. Upon completion, the mixture was filtered through a short pad of Celite, and the filtrate was concentrated under reduced pressure to afford the pure product, which required no further purification.

*[(η^5-C_5H_4-(1)-1,2,3-triazole-(4)CH_2-N=CH-(1)C_6H_4-(4)1H-1,2,4-triazole)Fe(η^5-C_5H_5)] (**2a**)*

This compound was prepared according to the general procedure described above, using in this case: [(η^5-C_5H_4-(1)-1,2,3-triazole-(4)CH_2-NH_2)Fe(η^5-C_5H_5)] (**1a**) (120 mg, 0.425 mmol) and 4-(1H-1,2,4-triazol-1-yl)benzaldehyde (74 mg, 0.425 mmol). Orange solid, yield 91% (169 mg, 0.387 mmol). FT-IR (KBr, cm^{-1}): 3132 (νCsp²–H); 1645 (νC=N); 1521 (νC=C); 1276 (νC–N). ^1H NMR (DMSO-d_6) δ 9.39 (s, 1H, 1,2,4-Triazole); 8.59 (s, 1H, CH=N); 8.48 (s, 1H, 1,2,3-Triazole); 8.27 (s, 1H, 1,2,4-Triazole); 7.97 (s, 4H, C_6H_4); 5.02 (t, J = 2.0 Hz, 2H, C_5H_4); 4.89 (s, 2H, CH_2); 4.33 (t, J = 2.0 Hz, 2H, C_5H_4); 4.20 (s, 5H, C_5H_5). Anal. (%) Calc. for $C_{22}H_{19}FeN_7$: C, 60.43; H, 4.38 and N, 22.42; found: C, 64.86; H, 4.70 and N, 23.84.

*[(η^5-C_5H_4-(1)-1,2,3-triazole-(4)CH_2-N=CH-(1)C_6H_4-(4)1H-1,2,4-triazole)Re$(CO)_3$] (**2b**)*

This compound was prepared according to the general procedure described above, using in this case: [(η^5-C_5H_4-(1)-1,2,3-triazole-(4)CH_2-NH_2)Re$(CO)_3$] (**1b**) (80 mg, 0.185 mmol) and 4-(1H-1,2,4-Triazol-1-yl)benzaldehyde (32 mg, 0.185 mmol). Brown solid, yield 87% (94 mg, 0.161 mmol). FT-IR (KBr, cm^{-1}): 3109 (νCsp²–H); 2028 (νRe-C=O); 1912 (νRe-C=O); 1654 (νC=N); 1520 (νC=C); 1261 (νC–N). ^1H NMR (DMSO-d_6) δ 9.39 (s, 1H, 1,2,4-Triazole); 8.57 (s, 2H, 1,2,3-Triazole/CH=N), 8.27 (s, 1H, 1,2,4-Triazole); 8.04 – 7.87 (m, 4H, C_6H_4); 6.56 (t, J = 2.4 Hz, 2H, C_5H_4); 5.80 (t, J = 2.4 Hz, 2H, C_5H_4); 4.89 (s, 2H, CH_2). Anal. (%) Calc. for $C_{20}H_{14}ReN_7O_3$: C, 40.95; H, 2.41 and N, 16.72; found: C, 46.88; H, 3.52 and N, 17.41.

2.4. Single Crystal X-ray diffraction measurements

For the **2a** compound, yellow block-shaped crystals suitable for single crystal X-ray diffraction (SC-XRD) analysis were obtained. A single crystal was mounted on a 75 µm MiTeGen loop and centered on a Bruker D8 Venture diffractometer equipped with a dual microfocus source. Data were collected using Mo Kα radiation (λ = 0.71073 Å). Unit cell determination, indexing, and data collection strategy were performed using the APEX5 program [37], while data integration and absorption corrections were applied with SADABS [38]. The structure was solved with SHELXT [39] using intrinsic phasing and refined by full-matrix least-squares methods on F^2 with SHELXL [40], both implemented within the Olex2 software. Hydrogen atoms were placed in calculated positions and refined with isotropic displacement parameters, whereas all non-hydrogen atoms were refined with anisotropic thermal parameters. ORTEP diagrams were generated using Olex2 [41].

3. RESULTS AND DISCUSSION

3.1. Synthesis and Characterization

The synthetic procedure to obtain compounds **1a**–**b** involved deprotection of the corresponding organometallic BOC-protected 1,2,3-triazoles (**P1** or **P2**) using excess trifluoroacetic acid (TFA) (**Scheme 1**). For compound **1b**, the remotion of TFA with subsequent DCM washing was found to be critical in preventing protonated species, which could lead to decrease yields in the next condensation steps. The synthesized compounds **1a**–**b** were obtained in good yields (95% for **1a**; 89% for **1b**) and exhibited distinct coloration: **1a** (orange), **1b** (green). These compounds demonstrated good solubility in common polar organic solvents (*e.g.* DCM, $CHCl_3$, MeOH, EtOH, DMSO, and CH_3CN) and remained air-stable, confirming their suitability for further study.

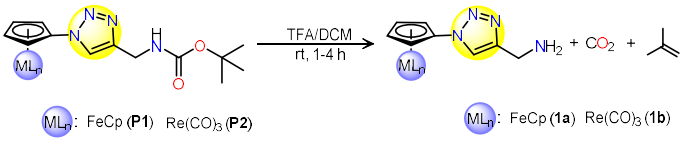

Scheme 1. Obtention of new organometallic aminomethyl 1,2,3-triazole.

For complete removal of the BOC protecting group in **1a**–**b**, different mixtures of TFA/DCM and MeOH/HCl at 5, 10, 25, and 50% were tested, with the best results observed at the highest concentration. For the ferrocene and cyrhetrene derivatives, TFA/DCM ratios of 25 and 50%, respectively, were employed. These rates showed only minor differences in the deprotection process, with no significant variation other than a slight difference in yield.

Initially, the structural identity of aminomethyl triazoles **1a**–**b** was confirmed by FT-IR spectroscopy. A key indication of successful BOC-group removal was the complete disappearance of the characteristic C=O stretching band (νC=O), observed at 1696 cm^{-1} for **P1** and 1688 cm^{-1} for **P2** in the spectra of their BOC-protected precursors (**Fig. S1–S2**†). Concomitantly, new absorption bands emerged in the 3225–3288 cm^{-1} region, consistent with N–H stretching vibrations of the free amino group generated upon deprotection (**Fig. S3–S4**†).

Additionally, the aminomethyl-substituted triazoles **1a**–**b** exhibited characteristic ν(Csp³–H) and ν(Csp²–H) stretching bands at 2936 cm^{-1} and 3134–3122 cm^{-1}, respectively. All compounds showed a medium-intensity absorption in the 1521–1527 cm^{-1} region, assignable to the C=C stretching mode of the triazole ring, confirming the integrity of the heterocycle formed through the [3+2] cycloaddition reaction. This spectral behavior is in good agreement with the data reported by Gamze Coz *et al.* for ferrocenyl–triazole hybrids derived from 18β-glycyrrhetinic acid [42].

Due to the incorporation of organometallic carbonyl moieties, compound **1b** displayed two intense absorption bands at 2028 and 1911 cm^{-1}, characteristic of Re–(C=O) stretching vibrations. Compared to the cyrhetrenyl-protected precursor **P2** (2029–1920 cm^{-1}), these bands exhibited slight shifts, reflecting the influence of the electronic nature of the substituent attached to the triazole ring. Specifically, electron-withdrawing groups, such as the carbonyl functionality of the BOC-protected amine, reduce the electron density on the triazole ring, thereby modulating the π-backbonding to the Re–carbonyl center. Similar behavior was reported by Toro *et al*. for 2-cyrhetrenyl-benzimidazoles [43].

The ^1H NMR analysis provided further evidence supporting the proposed structures (**Fig. S7**–**S8**†). The efficient removal of the BOC protecting group was confirmed by the disappearance of the characteristic tert-butyl and amide proton resonances from precursors **P1** and **P2** (1.40–1.39 and 7.41–7.37 ppm, respectively), accompanied by the appearance of signals for the free amine protons at 1.95 and 1.98 ppm for **1a** and **1b**. The spectra of compounds **1a–b** also revealed resonances characteristic of their respective organometallic fragments.

The ferrocenyl derivative **1a** exhibited two triplets at 5.00 and 4.34 ppm and a singlet at 4.22 ppm, whereas the cyrhetrenyl analogue **1b** showed two triplets at 6.54 and 5.81 ppm, corresponding to the substituted and unsubstituted cyclopentadienyl rings of the ferrocenyl and cyrhetrenyl moieties. Both compounds displayed a singlet at 3.80 ppm, assigned to the methylene protons (CH_2) adjacent to the triazole ring. The upfield shift of the methylene protons adjacent to the newly formed amine in comparation with **P1** and **P2** reflects the increased electron density and nucleophilic character of the $–CH_2NH_2$ functionality, underscoring its readiness for subsequent reactions. Additionally, the triazole proton appeared as a singlet at 8.33 ppm for **1a** and 8.43 ppm for **1b**. The slight downfield shift observed in **1b** ($\Delta\delta = 0.1$) reflects the opposite electronic effect relative to the cyrhetrenyl and ferrocenyl fragments [44].

3.2 Reactivity of organometallic aminomethyl 1,2,3-triazoles

The reactivity of the aminomethyl functionality in organometallic triazole derivatives **1a**–**b**, together with the potential influence of the electronic effects exerted by the organometallic fragments, it was investigated via condensation with 4-(1H-1,2,4-triazol-1-yl)benzaldehyde under mild conditions (DCM, rt). The reactions afforded the corresponding Schiff bases in excellent yields, **2a** (91%) and **2b** (87%), exhibiting distinct colors: **2a** (orange) and **2b** (brown) (**Scheme 2**). Both derivatives exhibited comparable behavior, as indicated by similar NH_2 proton shifts (1.98–1.95 ppm) and consistent conversions, confirming that the opposite electronic effects of the organometallic fragments do not play a significant role in the intrinsic reactivity of the $–CH_2NH_2$ group. This outcome demonstrates the efficiency of these systems for catalyst-free imine formation and their value as versatile platforms for constructing triazole-linked organometallic structures.

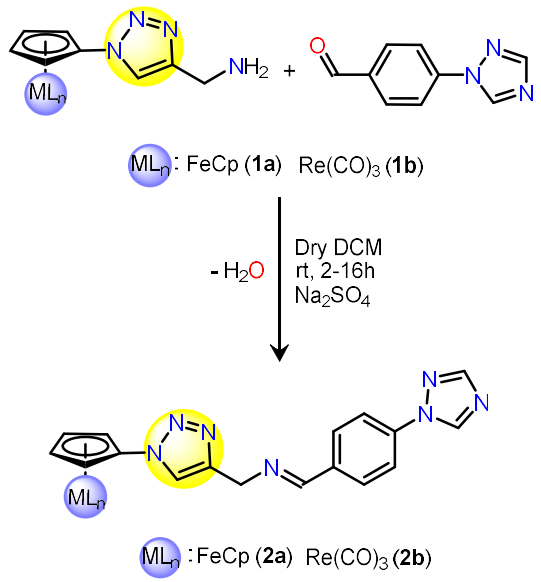

Scheme 2. Reactivity of **1a**–**b** in condensation reactions with 4-(1H-1,2,4-triazol-1-yl)benzaldehyde.

The successful formation of these compounds was confirmed first by FT-IR (**2a**–**b**) (**Fig. S5–S6**†), with the presence of the characteristic imine stretching band (C=N) at 1645 cm^{-1}, indicative of the imine bond. Moreover, additional absorption bands in the 1261–1276 cm^{-1} range were assigned to C–N stretching vibrations, consistent with the presence of imine within the molecular framework.

The formation of the new organometallic Schiff bases **2a**–**b** was confirmed by distinct spectral changes observed in the ^{1}H NMR spectra (**Fig. S9–S10**†). The signals corresponding to the free amine protons disappeared, consistent with conversion into the imine, while the methylene protons (CH_2) adjacent to the triazole shifted downfield from 3.80 ppm in **1a**–**b** to a doublet at 4.89 ppm in **2a**–**b**. The imine proton appeared at 8.48 ppm (**2a**) and 8.59 ppm (**2b**), confirming Schiff base formation. The ferrocenyl resonances in **2a** (5.03–4.20 ppm) remained largely unchanged from those of its aminomethyl precursor **1a** (5.15–4.22 ppm), indicating minimal perturbation of the ferrocene environment.

The triazole protons also shifted slightly downfield to 8.48 ppm (**2a**) and 8.57 ppm (**2b**), consistent with the electronic trends observed in the imine proton signals and aminomethyl analogues. In both cases, the ferrocenyl fragment acts as an electron-donating group, giving rise to higher-field resonances relative to the cyrhetrenyl analogue, where the electron-withdrawing $Re(CO)_3$ group induces slight deshielding. Comparable spectroscopic behaviors have been reported by Quintana and co-workers in related organometallic systems featuring sulfonamide linkages bridging ferrocene and cyrhetrene cores [45].

Finally, in both compounds (**2a**–**b**), the successful incorporation of the 4-(1H-1,2,4-triazol-1-yl)benzaldehyde fragment via Schiff base formation was evidenced by the spectral signals of the 1,4-disubstituted phenyl ring, appearing as a multiplet integrating for four protons at 7.97 ppm, and the 1,2,4-triazole ring, displaying two singlets at 9.39 and 8.27 ppm. These observations further underscore the high nucleophilicity of the terminal aminomethyl groups, which facilitates efficient and selective imine formation under mild conditions, confirming their utility for the controlled assembly of triazole-linked organometallic architectures.

3.3. Molecular structure of the 2a compound

The **2a** compound was crystallized from a dichloromethane/hexane 3:1 mixture of solvents, obtaining a single crystal suitable for single-crystal X-ray diffraction (SC-XRD) analysis**.** Crystallographic refinement parameters and general crystal data are summarized in **Table S1**†. Selected bond distances and angles are listed in **Tables S2–S3**†. The molecular structure with atom labeling is shown in **Figure 1**.

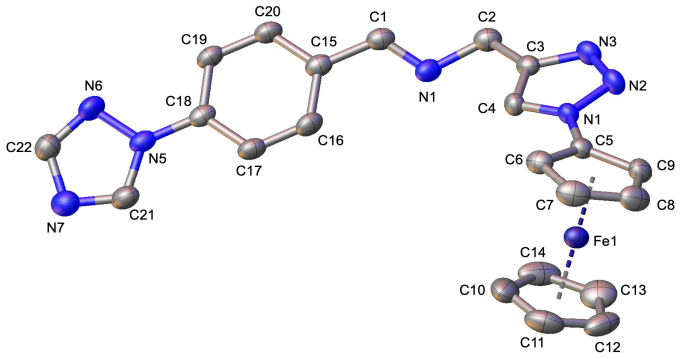

Figure 1. ORTEP diagram of the **2a** compound with thermal ellipsoids at the 30% probability. Hydrogen atoms omitted for clarity.

The organometallic molecule **2a** crystallizes in the centrosymmetric space group $P2_1/c$, with four molecular entities per unit cell ($Z = 4$; $Z' = 1$). The compound corresponds to a Schiff base containing a ferrocenyl 1*H*-1,2,3-triazole fragment connected through an azomethine bond (C1=N4) to an aromatic system that incorporates a 1*H*-1,2,4-triazole unit at the *-para* position of the phenyl ring. The configuration around the imine bond is *E*, as indicated by the coplanar torsion angle of 179.4(2)° for the four atoms (C2–N4–C1–C15) involved in the dihedral plane.

The 1*H*-1,2,3-triazole ring attached to the unsubstituted cyclopentadienyl (Cp) unit of the ferrocenyl core shows a deviation of *ca*. 26° from the Cp plane, whereas at the opposite end of the molecule, the 2*H*-1,2,4-triazole ring deviates by about 11° from the *para*-substituted phenyl moiety. The Fe–C and C–C bond lengths are consistent with reported ferrocenyl–1,2,3-triazole systems bearing direct Fe–N(triazole) linkage, showing no significant perturbation of the metallocene core [46]. Within the organometallic fragment, the substituted and unsubstituted cyclopentadienyl rings exhibit a tilt angle of 1.57(14)° and a twist angle of 5.7(3)° (N1–C5–Fe1–C14) confirming a nearly eclipsed conformation consistent with previous reports on ferrocenyl triazole amines [47].

The 1*H*-1,2,3-triazole ring shows uniform bond distances (N1–N2 = 1.348(2), N2–N3 = 1.316(3), N3–C3 = 1.352(3), C3–C4 = 1.361(3), and C4–N1 = 1.349(3) Å), suggesting π-delocalization. In contrast, the 2*H*-1,2,4-triazole ring displays bond length alternation between single and double bonds (N5–N6 = 1.356(3), N6–C22 = 1.296(4), C22–N7 = 1.348(3), N7–C21 = 1.307(4), and C21–N5 = 1.341(3) Å).

Weak nonclassical interactions of the C–H···N type is observed in the crystal packing (**Table 1**). The contacts C10–H10···N3[1], C21–H21···N6[2] and C22–H22···N7[3] show donor-acceptor distances in the range of 3.489(4) and 3.291(4) Å. The shortest interaction, C22–H22···N73, corresponds to an $R_2^2(6)$ ring motif, whereas the others as $C_1^1(7)$ [C10–H10···N3] and $C_1^1(4)$ [C21–H21···N6] chains arrangements, respectively. No significant π–π stacking interactions were found.

Table 1. Hydrogen-bond parameters (Å, °) for 2a.

D–H···A	d(D–H)/Å	d(H···A)/Å	d(D···A)/Å	(D–H···A)/°
C10–H10···N3[1]	0.93	2.75	3.489(4)	137.5
C21–H21···N6[2]	0.93	2.76	3.393(3)	126.3
C22–H22···N7[3]	0.93	2.48	3.291(4)	145.5
[1] 1 + x, 3/2 – y, 1/2 + z; [2] 2 – x, – 1/2 + y, 3/2 – z; [3] -x, 2 – y, 2 – z				

CONCLUSIONS

This work describes the synthesis of new aminomethyl-functionalized organometallic 1,2,3-triazoles, [(η⁵-C₅H₄-(1)-1,2,3-triazole-(4)-CH₂NH₂)MLn] [MLn = Fe(η⁵-C₅H₅) (**1a**), Re(CO)₃ (**1b**)], obtained via tert-butoxycarbonyl (BOC) deprotection in good yields (89–95%). Their structures were confirmed by FT-IR, ¹H NMR, and elemental analysis. The reactivity of these aminomethyl derivatives was then evaluated through condensation with 4-(1H-1,2,4-triazol-1-yl)benzaldehyde, affording the corresponding Schiff bases, [(η⁵-C₅H₄-(1)-1,2,3-triazole-(4)-CH₂N=CH-(1)-C₆H₄-(4)-1H-1,2,4-triazole)MLn] where [MLn = Fe(η⁵-C₅H₅) (**2a**), Re(CO)₃ (**2b**)], in good yields (87–91%) under mild conditions. Notably, it was not observed significant electronic influence from the organometallic fragment on the reactivity. Both compounds were fully characterized by spectroscopic and analytical techniques. Furthermore, the molecular structure of **2a**, determined by single-crystal X-ray diffraction, confirmed the incorporation of the phenyl-1,2,4-triazole fragment via the imine linkage, validating the proposed connectivity and organometallic framework. It is important to note that aminomethyl 1,2,3-triazoles serve as versatile organometallic precursors, enabling the construction of new Schiff base systems with potential applications in coordination and bioorganometallic chemistry.

ACKNOWLEDGEMENTS

This work was funded by the FONDECYT-Chile (Project # 1230296) and National Agency for Research and Development (ANID), NATIONAL DOCTORATE SCHOLARSHIPS (2021 – 21211253).

APPENDIX A. SUPPLEMENTARY MATERIAL

Electronic Supplementary Information (ESI) available: Characterization data and X-ray crystal structure determinations. CIF files containing tables of crystallographic parameters, bond distances, bond angles, as well as a list of structure factors deposited in the Cambridge Crystallographic Data Centre (CCDC 2498664 for **2a**). These data can be obtained free of charge via www.ccdc.cam.ac.uk/conts/retrieving.html; from the Cambridge Crystallographic Data Centre, 12 Union Road, Cambridge CB2 1EZ, UK; fax: (+44) 1223-336-033; or via e-mail: deposit@ccdc.cam.ac.uk.

REFERENCES

1. C. Elschenbroich, *Organometallics*, 3rd ed., Wiley-VCH, (2006)
2. R. H. Crabtree, *The Organometallic Chemistry of the Transition Metals*, 5th ed., John Wiley & Sons, (2009)
3. S. D. Pike; A. S. Weller, *Philos. Trans. R. Soc. A*, **373**, 20140187, (2015)
4. P. Omer; E. Abdulkareem; R. Omer; R. Faruq Rashid, *Rev. Inorg. Chem.*, **45**, 397, (2025)
5. G. Gasser; I. Ott; N. Metzler-Nolte, *J. Med. Chem.*, **54**, 3, (2011)
6. K. D. Mjøs; C. Orvig, *Chem. Rev.*, **114**, 4540, (2014)
7. M. Patra; G. Gasser, *Nat. Rev. Chem.*, **1**, 0066, (2017)
8. C. G. Hartinger; N. Metzler-Nolte; P. J. Dyson, *Organometallics*, **31**, 5677, (2012)
9. A. Leonidova; G. Gasser, *ACS Chem. Biol.*, **9**, 2180, (2014)
10. C. Ornelas; D. Astruc, *Pharmaceutics*, **15**, 2044, (2023)
11. T. Kealy; P. Pauson, *Nature*, **168**, 1039, (1951)
12. G. Wilkinson; M. Rosenblum; M. C. Whiting; R. B. Woodward, *J. Am. Chem. Soc.*, **74**, 2125, (1952)
13. H. Werner, *Angew. Chem. Int. Ed.*, **22**, 927, (1983)
14. J. Gómez; D. Sierra; M. Fuentealba; V. Artigas; A. H. Klahn, *J. Organomet. Chem.*, **883**, 65, (2019)
15. R. Arancibia; A. H. Klahn; G. E. Buono-Core; D. Contreras; G. Barriga; C. Olea-Azar; M. Lapier; J. D. Maya; A. Ibañez; M. T. Garland, *J. Organomet. Chem.*, **743**, 49, (2013)
16. C. Quintana; A. H. Klahn; V. Artigas; M. Fuentealba; C. Biot; I. Halloum; L. Kremer; R. Arancibia, *Inorg. Chem. Commun.*, **55**, 48, (2015)
17. T. Maldonado; G. Ferraudi; A. G. Lappin; F. Godoy, *J. Phys. Chem. A*, **123**, 9274, (2019)
18. R. Arancibia; A. H. Klahn; M. Lapier; J. D. Maya; A. Ibáñez; M. T. Garland; S. Carrère-Kremer; L. Kremer; C. Biot, *J. Organomet. Chem.*, **755**, 1, (2014)
19. V. V. Rostovtsev; L. G. Green; V. V. Fokin; K. B. Sharpless, *Angew. Chem. Int. Ed.*, **41**, 2596, (2002)
20. L. Liang; D. Astruc, *Coord. Chem. Rev.*, **255**, 2933, (2011)
21. V. Ganesh; V. S. Sudhir; T. Kundu; S. Chandrasekaran, *Chem. Asian J.*, **6**, 2670, (2011)
22. B. Beyer; C. Ulbricht; D. Escudero; C. Friebe; A. Winter; L. González; U. S. Schubert, *Organometallics*, **28**, 5478, (2009)
23. F. Saleem; G. K. Rao; A. Kumar; G. Mukherjee; A. K. Singh, *Organometallics*, **32**, 3595, (2013)
24. D. P. Day; T. Dann; R. J. Blagg; G. G. Wildgoose, *J. Organomet. Chem.*, **770**, 29, (2014)
25. P. Biegański; E. Kovalski; N. Israel; E. Dmitrieva; D. Trzybiński; K. Woźniak; V. Vrček; M. Godel; C. Riganti; J. Kopecka; H. Lang; K. Kowalski, *Inorg. Chem.*, **61**, 9650, (2022)
26. D. Coelho; Y. Colas; M. Ethève-Quelquejeu; E. Braud; L. Iannazzo, *ChemBioChem*, **25**, e202400150, (2024)
27. J. Ceramella; D. Iacopetta; A. Catalano; F. Cirillo; R. Lappano; M. S. Sinicropi, *Antibiotics (Basel).*, **11**, 191, (2022)
28. R. Aggarwal; G. Sumran, *Eur. J. Med. Chem.*, **205**, 112652, (2020)
29. O. Guerret; S. Solé; H. Gornitzka; G. Trinquier; G. Bertrand, *J. Organomet. Chem.*, **600**, 112, (2000)
30. J. Liu; L. Li; H. Dai; Z. Liu; J. Fang, *J. Organomet. Chem.*, **691**, 2686, (2006)
31. B. D. Sadanala; R. Trivedi, *Chem. Rec.*, **24**, e202300347, (2024)
32. H. S. Scott; A. Nafady; J. D. Cashion; A. M. Bond; B. Moubaraki; K. S. Murray; S. M. Neville, *Dalton Trans.*, **42**, 10168, (2013)
33. Z. Jin; A. Huo; T. Liu; Y. Hu; J. Liu; J. Fang, *J. Organomet. Chem.*, **690**, 1226, (2005)
34. K. Yin; Y. Ruan; M. Guo; Q. Tang; F. Nie; Y. Wang; H. Guo; Y. Wang; S. Zhou; D. Yang; Y. Tang; R. Jin; H. Peng, *Bioorg. Chem.*, **165**, 108936, (2025)
35. Manuscript submitted to *J. Organomet. Chem.*, (submitted)
36. W. L. F. Armarego; C. L. L. Chai, *Purification of Laboratory Chemicals*, 5th ed., Butterworth-Heinemann, (2003)
37. Bruker. APEX5. Bruker AXS Inc., Madison, Wisconsin, USA, (2023)
38. G. M. Sheldrick, *SADABS*, Program for Empirical Absorption Correction of Area Detector Data, (1996)
39. G. M. Sheldrick, *Acta Crystallogr.*, A71, 3, (2015)
40. G. M. Sheldrick, *Acta Crystallogr.*, C71, 3, (2015)
41. O. V. Dolomanov; L. J. Bourhis; R. J. Gildea; J. A. K. Howard; H. Puschmann, *J. Appl. Crystallogr.*, **42**, 339, (2009)
42. Z. Öztürk; Y. Yıldız; N. Abul; O. Ertik; F. Arı; İ. Gülçin; Ö. Koz; G. Koz, *Polyhedron.*, **279**, 117620, (2025)
43. P. Toro; A. H. Klahn; B. Pradines; F. Lahoz; A. Pascual; C. Biot; R. Arancibia, *Inorg. Chem. Commun.*, **35**, 126, (2013)
44. Y. Huentupil; L. Peña; N. Novoa; E. Berrino; R. Arancibia; C. T. Supuran, *J. Enzyme Inhib. Med. Chem.*, **34**, 451, (2019)
45. C. Quintana; G. Silva; A. H. Klahn; V. Artigas; M. Fuentealba; C. Biot; I. Halloum; L. Kremer; N. Novoa; R. Arancibia, *Polyhedron.*, **134**, 166, (2017)
46. F. Otón; M. del C. González; A. Espinosa; A. Tárraga; P. Molina, *Organometallics*, **31**, 1758, (2012)
47. K. Al Khalyfeh; A. Ghazzy; R. M. Al-As' Ad; T. Rüffer; O. Kanoun; H. Lang, *RSC Adv.*, **14**, 20572, (2024)

SUPPORTING INFORMATION FOR

Organometallic Aminomethyl 1,2,3-Triazoles: Synthesis, Characterization and Reactivity

Luis Peña [a], David Villaman [a], Rodrigo Arancibia [a*]

[a] Facultad de Ciencias Químicas, Universidad de Concepción, Concepción, Chile.

e-mail: rarancibia@udec.cl

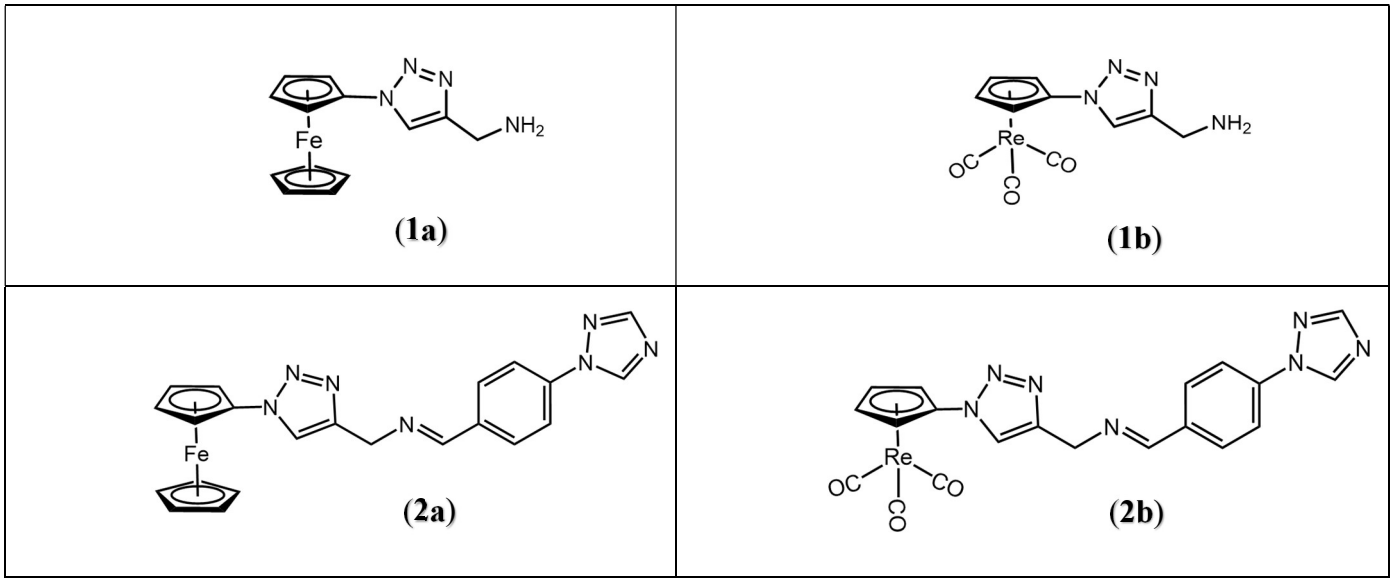

Supporting information contents:

1.- Supplementary Figures:

Fig. S1. FT-IR spectrum (KBr pellet) of compound **P1**.

Fig. S2. FT-IR spectrum (KBr pellet) of compound **P2**.

Fig. S3. FT-IR spectrum (KBr pellet) of compound **1a**.

Fig. S4. FT-IR spectrum (KBr pellet) of compound **1b**.

Fig. S5. FT-IR spectrum (KBr pellet) of compound **2a**.

Fig. S6. FT-IR spectrum (KBr pellet) of compound **2b**.

Fig. S7. ^{1}H NMR spectrum (400 MHz) of compound **1a** in DMSO-d_6 at 298 K.

Fig. S8. ^{1}H NMR spectrum (400 MHz) of compound **1b** in DMSO-d_6 at 298 K.

Fig. S9. ^{1}H NMR spectrum (400 MHz) of compound **2a** in DMSO-d_6 at 298 K.

Fig. S10. ^{1}H NMR spectrum (400 MHz) of compound **2b** in DMSO-d_6 at 298 K.

2.- Supplementary Tables:

Table S1. Crystal data and structure refinement for **2a**.

Table S2. Selected bond lengths (Å) for **2a.**

Table S3. Selected bond angles (°) for **2a.**

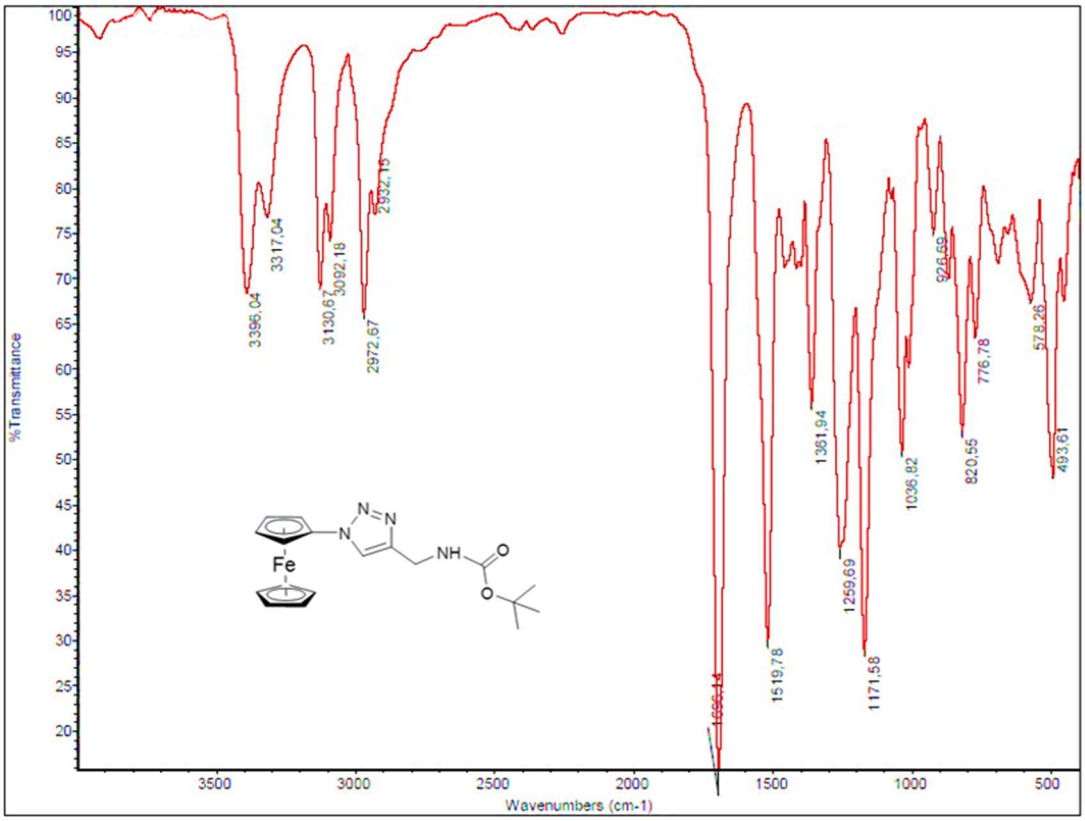

Fig. S1. FT-IR spectrum (KBr pellet) of compound **P1**.

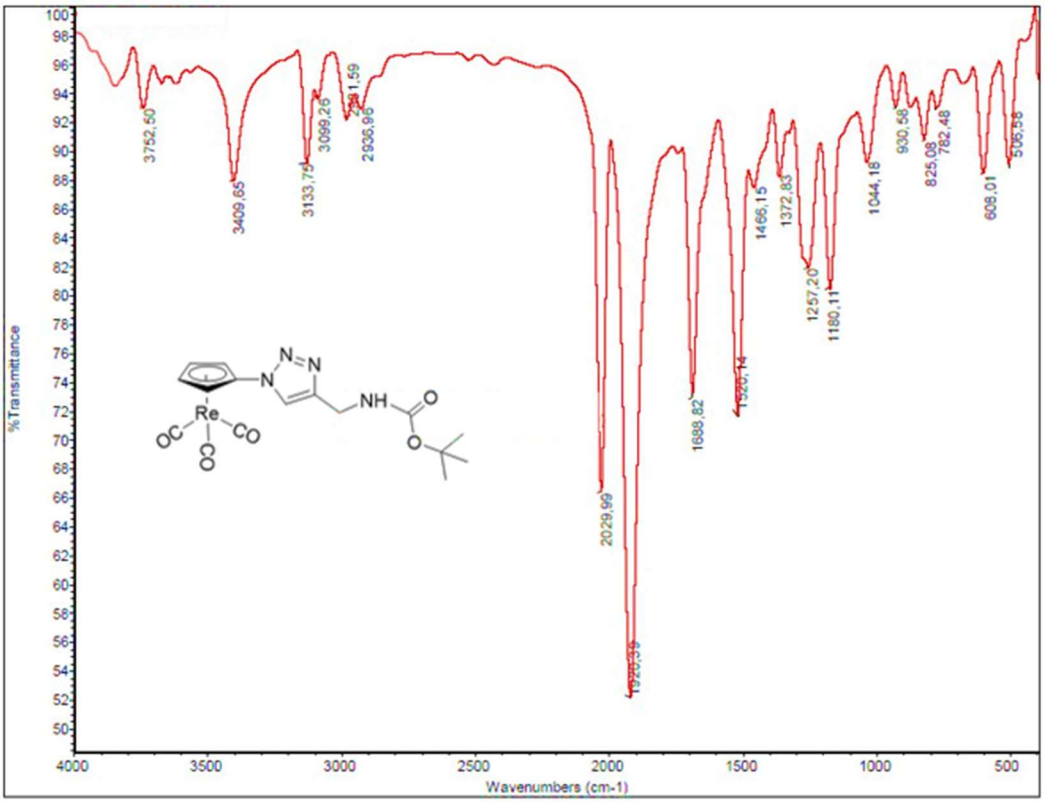

Fig. S2. FT-IR spectrum (KBr pellet) of compound **P2**.

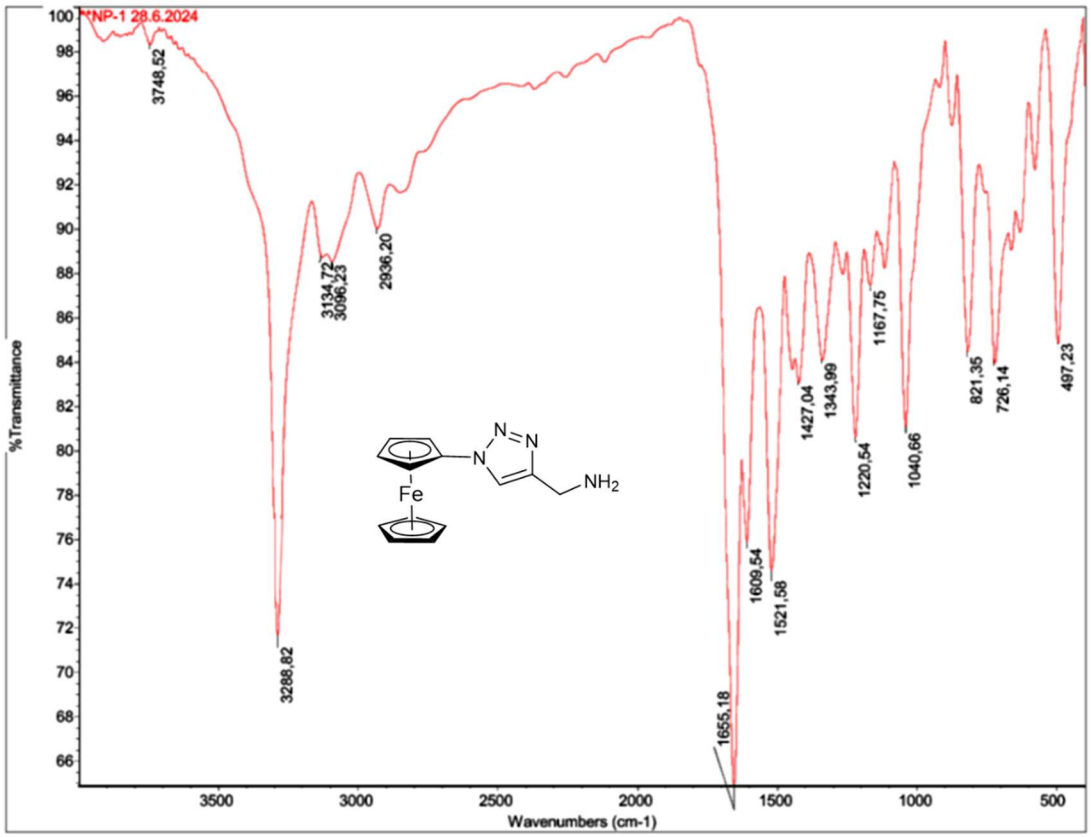

Fig. S3. FT-IR spectrum (KBr pellet) of compound **1a**.

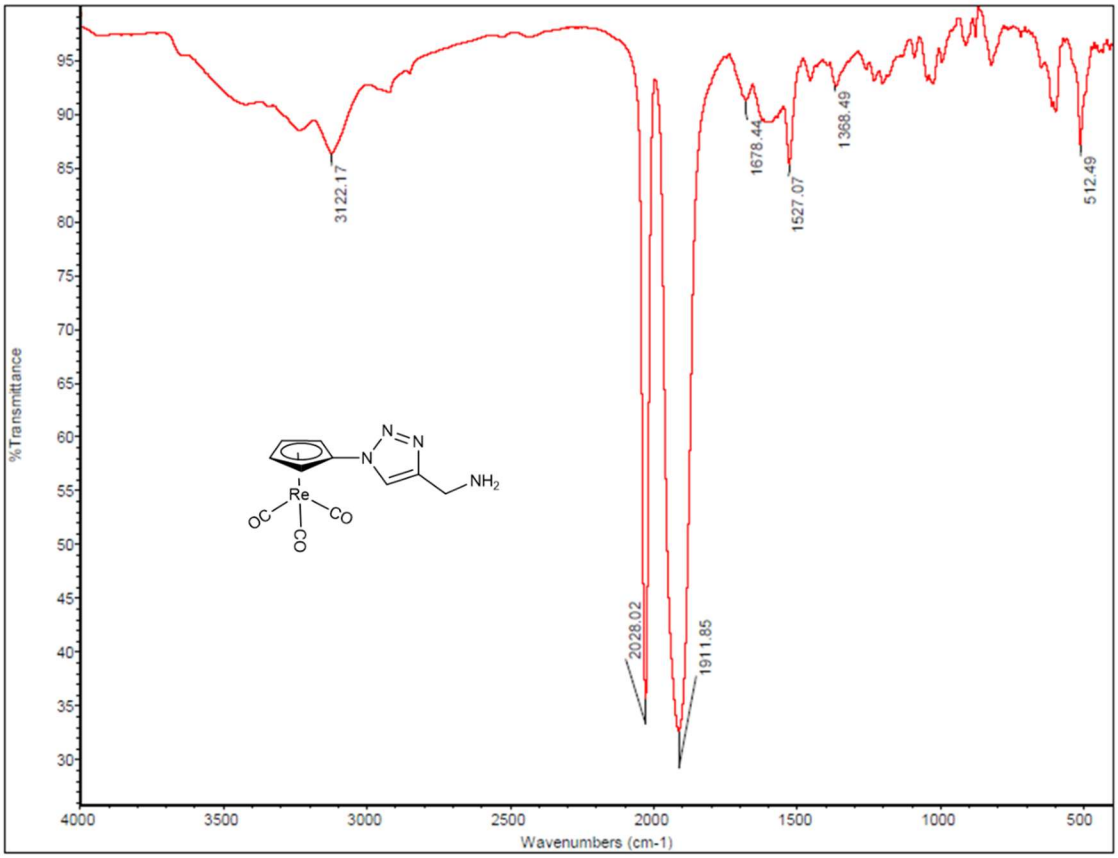

Fig. S4. FT-IR spectrum (KBr pellet) of compound **1b**.

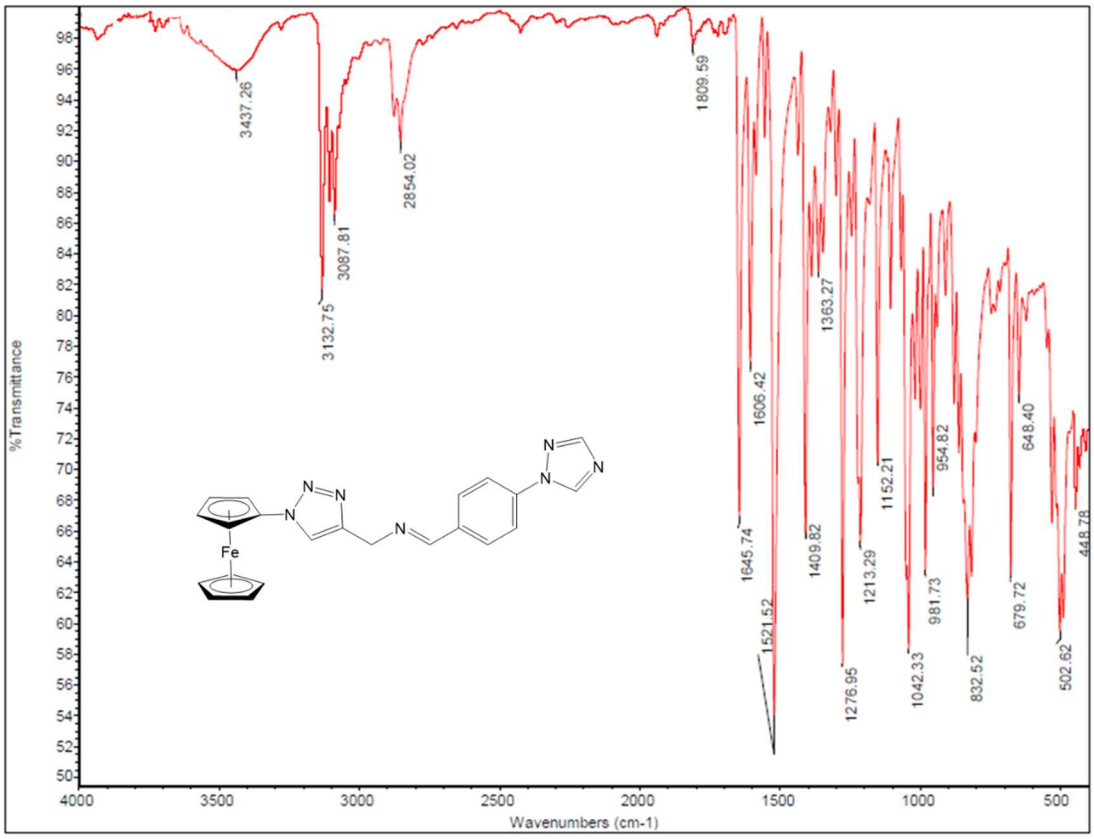

Fig. S5. FT-IR spectrum (KBr pellet) of compound **2a**.

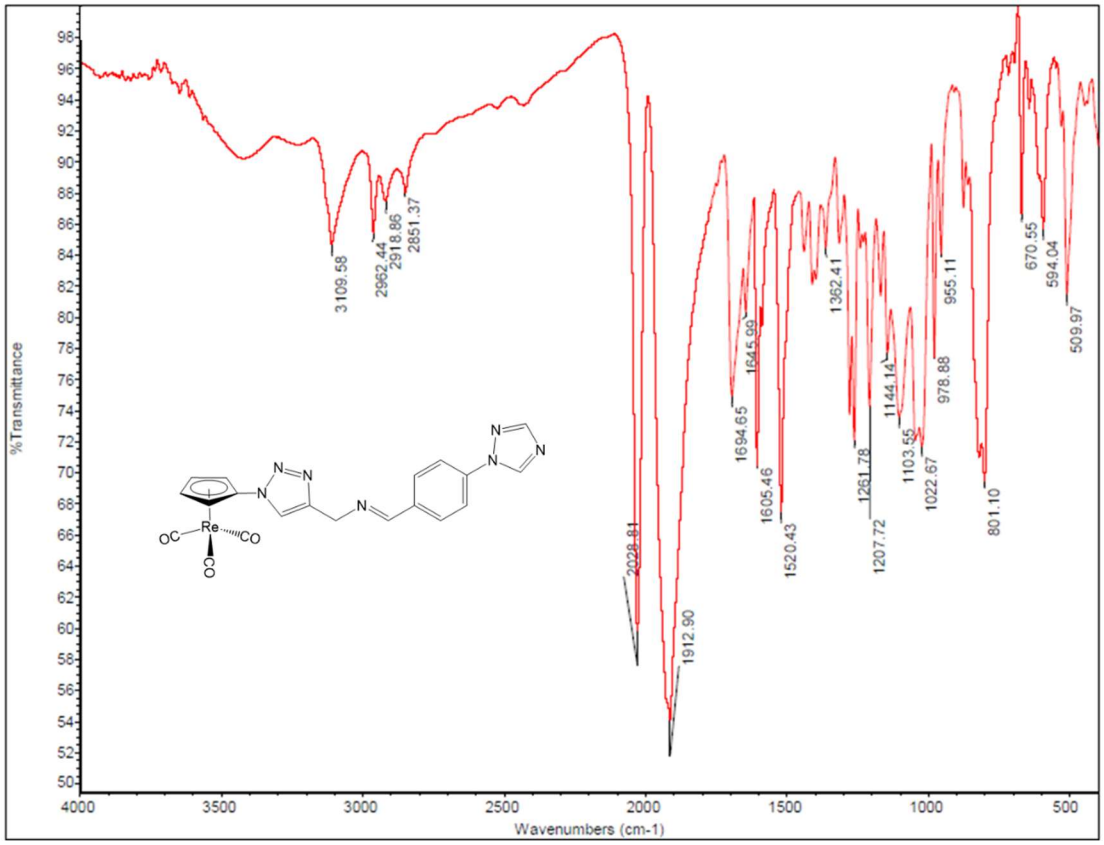

Fig. S6. FT-IR spectrum (KBr pellet) of compound **2b**.

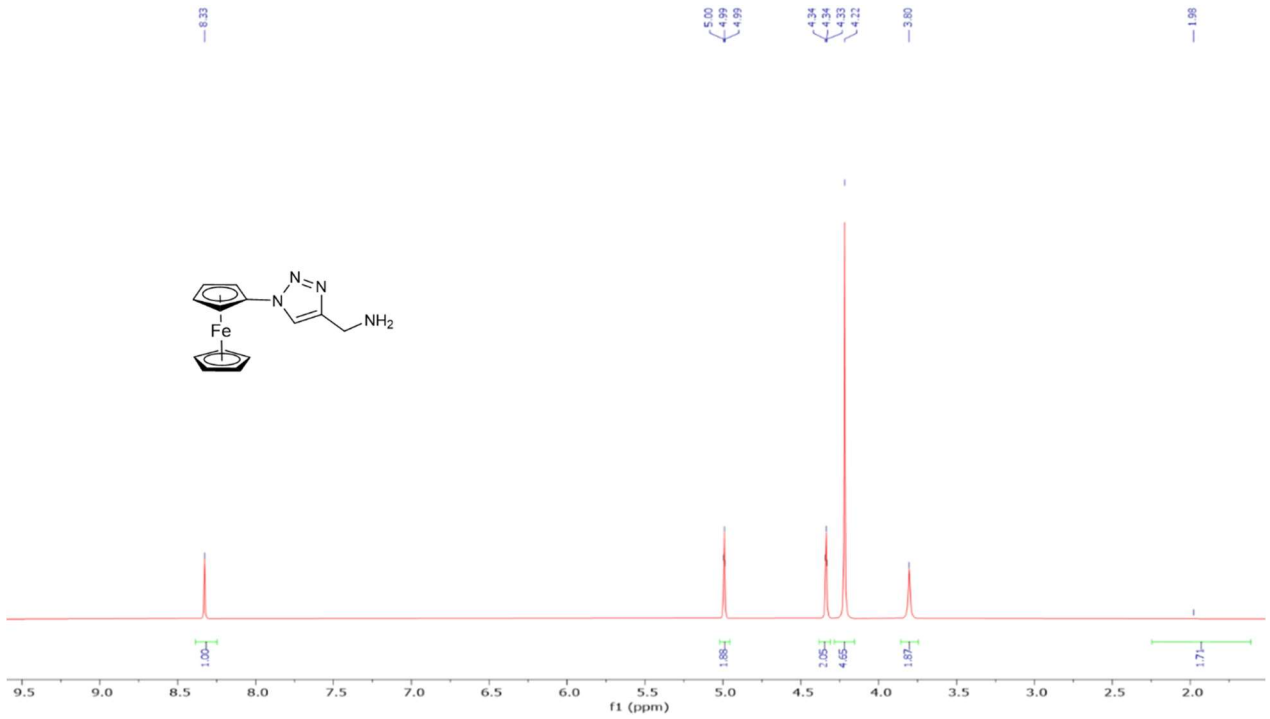

Fig. S7. ^{1}H NMR spectrum (400 MHz) of compound **1a** in DMSO-d_6.

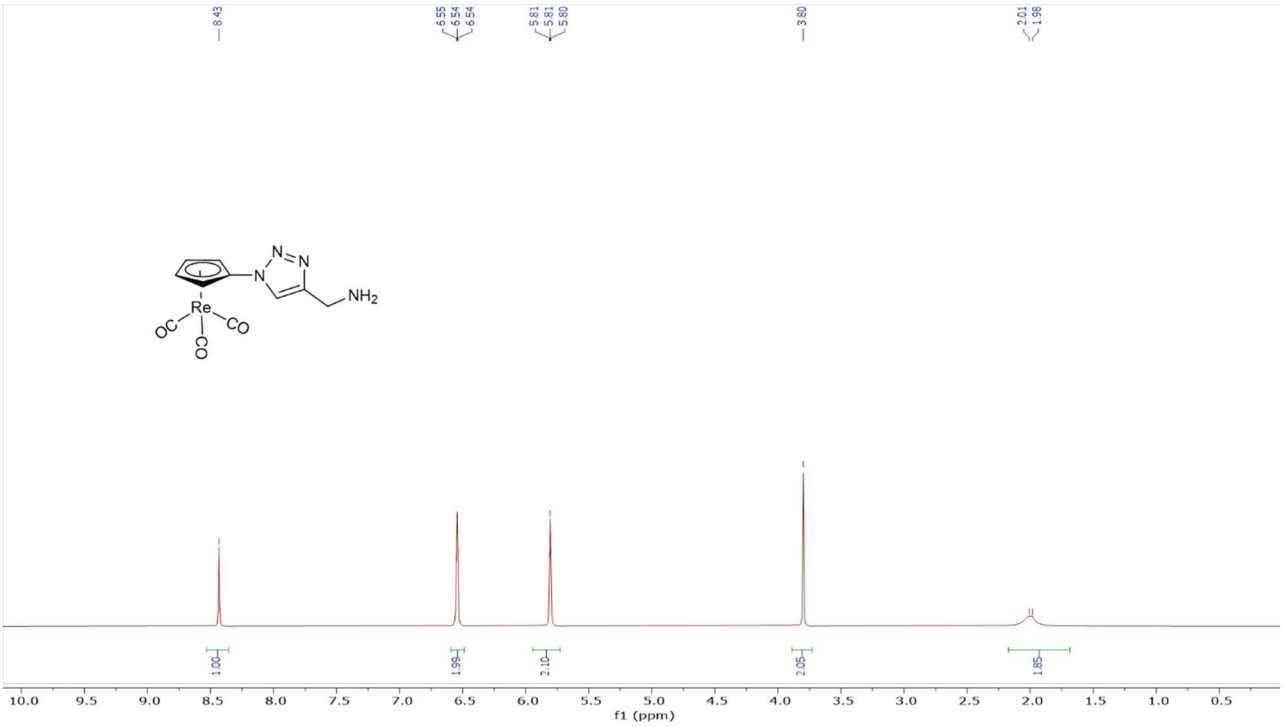

Fig. S8. ^{1}H NMR spectrum (400 MHz) of compound **1b** in DMSO-d_6.

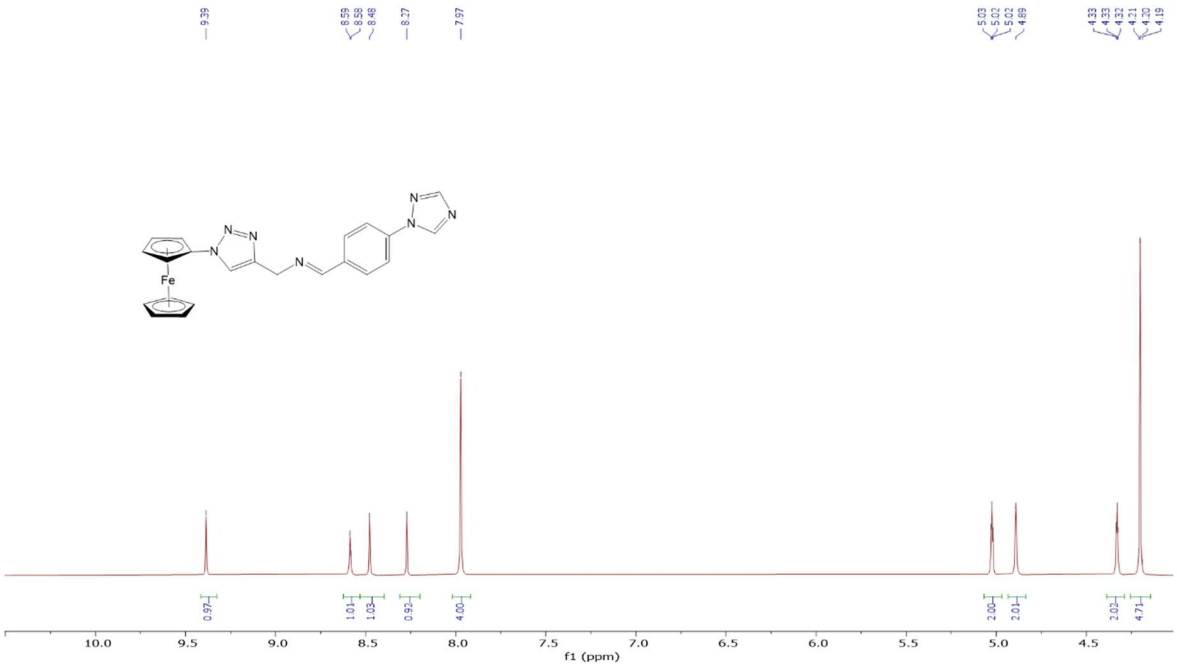

Fig. S9. ^{1}H NMR spectrum (400 MHz) of compound **2a** in DMSO-d_6.

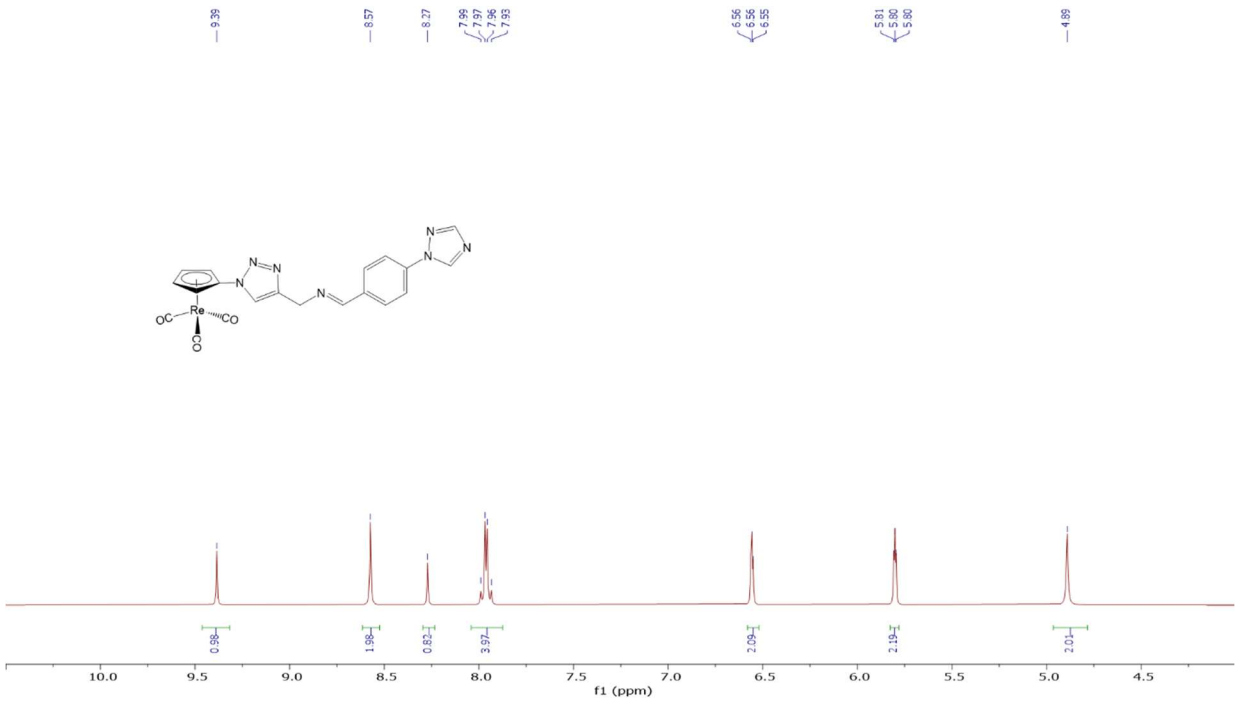

Fig. S10. ^{1}H NMR spectrum (400 MHz) of compound **2b** in DMSO-d_6.

Table S1. Crystal data and structure refinement for **2a**.

Empirical formula	$C_{22}H_{19}FeN_7$
Formula weight	437.29
Temperature/K	296.15
Crystal system	monoclinic
Space group	$P2_1/c$
a/Å	18.1423(5)
b/Å	10.1970(2)
c/Å	11.1261(3)
α/°	90
β/°	104.3900(10)
γ/°	90
Volume/Å³	1993.72(9)
Z	4
ρ_{calc}g/cm³	1.457
μ/mm⁻¹	0.781
F(000)	904.0
Crystal size/mm³	0.13 × 0.11 × 0.08
Radiation	Mo Kα (λ = 0.71073)
2Θ range for data collection/°	4.618 to 54.254
Index ranges	-23 ≤ h ≤ 23, -13 ≤ k ≤ 13, -14 ≤ l ≤ 14
Reflections collected	47132
Independent reflections	4408 [R_{int} = 0.0750, R_{sigma} = 0.0337]
Data/restraints/parameters	4408/0/271
Goodness-of-fit on F²	1.042
Final R indexes [I>=2σ (I)]	R_1 = 0.0413, wR_2 = 0.1047
Final R indexes [all data]	R_1 = 0.0611, wR_2 = 0.1172
Largest diff. peak/hole / e Å⁻³	0.27/-0.20

Table S2. Selected bond lengths (Å) for **2a.**

Atoms	Length/Å	Atoms	Length/Å
Fe1–C5	2.031(2)	**N5–C18**	1.418(3)
Fe1–C6	2.039(2)	**N5–C21**	1.341(3)
Fe1–C7	2.031(3)	**C5–C6**	1.423(3)
Fe1–C8	2.038(3)	**C5–C9**	1.413(3)
Fe1–C9	2.047(2)	**N6–C22**	1.296(4)
Fe1–C10	2.028(3)	**C6–C7**	1.417(4)
Fe1–C11	2.030(3)	**N7–C21**	1.307(4)
Fe1–C12	2.034(3)	**N7–C22**	1.348(3)
Fe1–C13	2.032(3)	**C7–C8**	1.406(4)
Fe1–C14	2.020(3)	**C8–C9**	1.410(4)
N1–N2	1.348(2)	**C10–C11**	1.397(5)
N1–C4	1.349(3)	**C10–C14**	1.392(5)
N1–C5	1.413(3)	**C11–C12**	1.388(5)
C1–N4	1.259(3)	**C12–C13**	1.380(5)
C1–C15	1.469(4)	**C13–C14**	1.376(5)
N2–N3	1.316(3)	**C15–C16**	1.393(3)
C2–C3	1.496(3)	**C15–C20**	1.395(3)
C2–N4	1.464(3)	**C16–C17**	1.363(4)
N3–C3	1.352(3)	**C17–C18**	1.386(3)
C3–C4	1.361(3)	**C18–C19**	1.386(3)
N5–N6	1.356(3)	**C19–C20**	1.377(4)

Table S3. Selected bond angles (°) for **2a.**

Atoms	Angle/°	Atoms	Angle/°
C5–Fe1–C6	40.93(9)	**C4–C3–C2**	130.1(2)
C5–Fe1–C8	67.77(10)	**C1–N4–C2**	117.6(2)
C5–Fe1–C9	40.55(9)	**N1–C4–C3**	104.93(19)
C5–Fe1–C12	155.45(15)	**N6–N5–C18**	121.80(19)
C5–Fe1–C13	121.27(13)	**C21–N5–N6**	107.7(2)
C6–Fe1–C9	68.85(11)	**C21–N5–C18**	130.4(2)
C7–Fe1–C5	68.25(10)	**N1–C5–Fe1**	128.99(15)
C7–Fe1–C6	40.74(11)	**N1–C5–C6**	125.9(2)
C7–Fe1–C8	40.45(12)	**C6–C5–Fe1**	69.80(13)
C7–Fe1–C9	68.41(12)	**C9–C5–Fe1**	70.32(13)
C7–Fe1–C12	126.56(13)	**C9–C5–N1**	125.0(2)
C7–Fe1–C13	163.68(15)	**C9–C5–C6**	109.1(2)
C8–Fe1–C6	68.31(12)	**C22–N6–N5**	103.1(2)
C8–Fe1–C9	40.39(11)	**C5–C6–Fe1**	69.27(13)
C10–Fe1–C5	126.08(12)	**C7–C6–Fe1**	69.33(15)
C10–Fe1–C6	107.02(13)	**C7–C6–C5**	106.7(2)
C10–Fe1–C7	119.62(17)	**C21–N7–C22**	101.7(2)
C10–Fe1–C8	154.52(17)	**C6–C7–Fe1**	69.93(14)
C10–Fe1–C9	163.47(15)	**C8–C7–Fe1**	70.04(16)
C10–Fe1–C11	40.29(15)	**C8–C7–C6**	108.3(2)
C10–Fe1–C12	67.26(14)	**C7–C8–Fe1**	69.51(16)
C10–Fe1–C13	67.27(17)	**C7–C8–C9**	109.0(2)
C11–Fe1–C5	163.06(15)	**C9–C8–Fe1**	70.17(15)
C11–Fe1–C6	125.38(14)	**C5–C9–Fe1**	69.13(13)
C11–Fe1–C7	107.75(14)	**C8–C9–Fe1**	69.44(15)
C11–Fe1–C8	120.64(14)	**C8–C9–C5**	106.9(2)
C11–Fe1–C9	154.99(14)	**C11–C10–Fe1**	69.91(19)
C11–Fe1–C12	39.93(15)	**C14–C10–Fe1**	69.58(19)
C11–Fe1–C13	67.08(16)	**C14–C10–C11**	107.1(3)
C12–Fe1–C6	162.86(14)	**C10–C11–Fe1**	69.80(18)
C12–Fe1–C8	109.42(13)	**C12–C11–Fe1**	70.20(18)
C12–Fe1–C9	121.23(14)	**C12–C11–C10**	107.8(3)
C13–Fe1–C6	154.96(13)	**C11–C12–Fe1**	69.86(18)
C13–Fe1–C8	127.45(15)	**C13–C12–Fe1**	70.11(18)
C13–Fe1–C9	109.28(14)	**C13–C12–C11**	108.4(3)
C13–Fe1–C12	39.67(14)	**C12–C13–Fe1**	70.22(18)
C14–Fe1–C5	108.75(11)	**C14–C13–Fe1**	69.67(19)
C14–Fe1–C6	120.13(14)	**C14–C13–C12**	108.1(4)
C14–Fe1–C7	154.49(17)	**C10–C14–Fe1**	70.19(19)
C14–Fe1–C8	163.94(18)	**C13–C14–Fe1**	70.62(18)
C14–Fe1–C9	126.84(15)	**C13–C14–C10**	108.6(3)
C14–Fe1–C10	40.24(16)	**C16–C15–C1**	121.2(2)
C14–Fe1–C11	67.32(14)	**C16–C15–C20**	118.2(2)
C14–Fe1–C12	66.78(13)	**C20–C15–C1**	120.5(2)
C14–Fe1–C13	39.71(15)	**C17–C16–C15**	121.1(2)
N2–N1–C4	110.71(18)	**C16–C17–C18**	120.0(2)
N2–N1–C5	119.15(18)	**C17–C18–N5**	119.8(2)
C4–N1–C5	130.11(18)	**C17–C18–C19**	120.3(2)
N4–C1–C15	121.8(2)	**C19–C18–N5**	119.9(2)
N3–N2–N1	106.61(18)	**C20–C19–C18**	119.2(2)
N4–C2–C3	109.9(2)	**C19–C20–C15**	121.2(2)
N2–N3–C3	109.30(18)	**N7–C21–N5**	111.7(2)
N3–C3–C2	121.4(2)	**N6–C22–N7**	115.7(3)
N3–C3–C4	108.4(2)		